GLOBAL MHD SIMULATIONS OF SPACE PLASMA ENVIRONMENTS: HELIOSPHERE, COMETS, MAGNETOSPHERES OF PLANETS AND SATELLITES

K. KABIN, K.C. HANSEN, T.I. GOMBOSI, M.R. COMBI, T.J. LINDE⋆, D.L. DEZEEUW, C.P.T. GROTH⋆⋆, K.G. POWELL and A.F. NAGY

University of Michigan

Abstract. Magnetohydrodynamics (MHD) provides an approximate description of a great variety of processes in space physics. Accurate numerical solutions of the MHD equations are still a challenge, but in the past decade a number of robust methods have appeared. Once these techniques made the direct solution of MHD equations feasible, a number of global three-dimensional models were designed and applied to many space physics objects. The range of these objects is truly astonishing, including active galactic nuclei, the heliosphere, the solar corona, and the solar wind interaction with planets, satellites, and comets. Outside the realm of space physics, MHD theory has been applied to such diverse problems as laboratory plasmas and electromagnetic casting of liquid metals. In this paper we present a broad spectrum of models of different phenomena in space science developed in the recent years at the University of Michigan. Although the physical systems addressed by these models are different, they all use the MHD equations as a unifying basis.

1. Mathematical Basis of the Models

The global models that we are presenting here are based on a recently developed code that solves the ideal MHD equations. It is understood that these equations represent a simplified description of the physics involved in space science applications, for example, they neglect kinetic effects, ignore resistivity and diffusion, and treat the ions and electrons as a single fluid. The main benefit of solving the MHD equations is that they are simple enough to be solved over a large domain with a reasonable amount of computing resources, while at the same time being realistic enough that models lead to correct physical insights. Below we outline the MHD equations and the numerical method used to solve them.

The ideal MHD equations are:

$$\frac{\partial \mathbf{W}}{\partial t} + (\nabla \cdot \mathbf{F}) = \mathbf{S} - \mathbf{L} \tag{1}$$

⋆ Now at University of Chicago
⋆⋆ Now at University of Toronto

where $\mathbf{W}$, $\mathbf{S}$ and $\mathbf{L}$ are the eight-dimensional state, source, and loss vectors, respectively, and $\mathbf{F}$ is an 8×3 dimensional flux tensor. The normalized state vector and flux tensor are

$$\mathbf{W} = \begin{pmatrix} \rho \\ \rho\,\mathbf{u} \\ \mathbf{B} \\ \varepsilon \end{pmatrix} \tag{2}$$

$$\mathbf{F} = \begin{pmatrix} \rho\,\mathbf{u} \\ \rho\,\mathbf{u}\,\mathbf{u} + \left(p + \frac{B^2}{2\mu_0}\right)\mathbf{I} - \frac{\mathbf{B}\mathbf{B}}{\mu_0} \\ \mathbf{u}\mathbf{B} - \mathbf{B}\mathbf{u} \\ \mathbf{u}\left(\frac{1}{2}\rho\,u^2 + \frac{\gamma}{\gamma-1}p + \frac{B^2}{\mu_0}\right) - \frac{(\mathbf{B}\cdot\mathbf{u})\,\mathbf{B}}{\mu_0} \end{pmatrix} \tag{3}$$

were total energy density, ϵ, is given by

$$\epsilon = \frac{1}{2}\rho u^2 + \frac{1}{\gamma-1}p + \frac{B^2}{2\mu_0} \tag{4}$$

and the source and loss terms are given by

$$\mathbf{S} = \dot{\rho} \begin{pmatrix} 1 \\ \mathbf{u}_n + \eta\rho\,(\mathbf{u}_n - \mathbf{u}) \\ \mathbf{0} \\ \frac{1}{2}\left[u_n^2 + \eta\rho\,(u_n^2 - u^2) - 3\eta\rho\right] \end{pmatrix} \tag{5}$$

$$\mathbf{L} = \mathcal{L}_e \begin{pmatrix} \rho \\ \rho\mathbf{u} \\ \mathbf{0} \\ \frac{1}{2}\rho u^2 + \frac{3}{2}p \end{pmatrix} \tag{6}$$

where t, $\mathbf{r}$, ρ, $\mathbf{u}$, p, and $\mathbf{B}$ represent time, radius vector, mass density, bulk flow velocity, pressure and magnetic field respectively. The subscript 'n' refers to the neutral particles, $\dot{\rho}$ is the mass addition rate, η is the ion-neutral friction coefficient and $\mathcal{L}_e$ is the mass loss coefficient due to electron-ion recombination.

Equation (1) describes the transport of mass, momentum, magnetic flux, and total energy density. The terms on the right hand side, $\mathbf{S}$ and $\mathbf{L}$, represent source and loss terms due to ionization, charge exchange and recombination. These terms are different depending on the space environment. The derivation of the above form for the source and loss terms can be found, for example, in Gombosi et al. (1996).

Equation (1) is solved by using an explicit, high-resolution Godunov-type scheme based on an approximate Riemann solver for magnetohydrodynamics (Powell et al., 1999). The code uses a limited reconstruction that achieves second-order accuracy away from discontinuities, while simultaneously ensuring non-oscillatory

solutions. Our model uses an unstructured Cartesian block-adaptive grid, which allows an effective implementation on a massively parallel computer (Stout *et al.*, 1997; Groth *et al.*, 1999).

2. Heliosphere

Our simulation of the heliosphere is a slightly improved version of Linde *et al.* (1998) and Linde (1998). We differentiate between slow and fast solar winds and include the direction of the interstellar magnetic field, consistent with observations (Frisch, 1996). At the same time, there are clearly many aspects of the model which should be improved in the future. For example, we treat neutral hydrogen as a fluid, while a kinetic description is more appropriate (Baranov *et al.*, 1998).

We define a coordinate system in such a way that the x-axis points in the direction opposite to the direction of relative motion of the Sun and the interstellar media, the y-axis lies in the equatorial plane and the z-axis points northward along the rotational axis of the Sun. In this coordinate system the interstellar magnetic field direction is given by (0.322, 0.541, 0.777). In our computations we chose to put the inner boundary at 30 AU which roughly coincides with the orbit of Neptune. At this heliocentric distance we prescribe the following solar wind parameters (corresponding to solar minimum): $n_p v_p = 3.5 \times 10^9$ m^{-2} s^{-1}, $n_p^{\text{slow}} = 7.8 \times 10^3$ m^{-3}, $n_p^{\text{fast}} = 4.5 \times 10^3$ m^{-3}, $n_\alpha = 0.045 \, n_p$, $v_p^{\text{slow}} = 450$ km s^{-1}, $v_p^{\text{fast}} = 780$ km s^{-1}, $T_p = 3 \times 10^4$ K, $B = 0.2$ nT. We have placed the boundary between slow and fast solar winds at 30° latitude. For the Local Interstellar Medium (LISM) we adopt the following parameters: $n_p = 7 \times 10^4$ m^{-3}, $n_{\text{H}} = 2 \times 10^5$ m^{-3}, $n_{\text{He}^+} = 9 \times 10^3$ m^{-3}, $v_p = 26$ km s^{-1}, $T_p = 7500$ K, $B = 0.15$ nT.

Figure 1 presents the contours of magnetic field intensity in the north-south meridional plane. The interplanetary magnetic field has different polarities in the northern and southern hemispheres, therefore its interaction with the interstellar magnetic field must be different in the two hemispheres. During the 1996 solar minimum, which we model, the azimuthal components of the two fields at the nose of the heliopause had different signs in the northern hemisphere and same signs in the southern one. This situation is reflected in Figure 1 in which a pronounced drop of magnetic field intensity is visible in the northern hemisphere. The southern hemisphere, on the other hand, features a very strong (for the outer heliosphere) magnetic field that reaches values as high as 0.7 nT.

The heliopause, being a magnetic discontinuity, must also be a current surface. The strength of a current sheet is proportional to the magnetic field jump across it, therefore, it is clear that heliopause currents in the northern hemisphere must be stronger than they are in the southern one. It is not therefore surprising to see in Figure 1 that the heliospheric current sheet connects to the northern part of the heliopause.
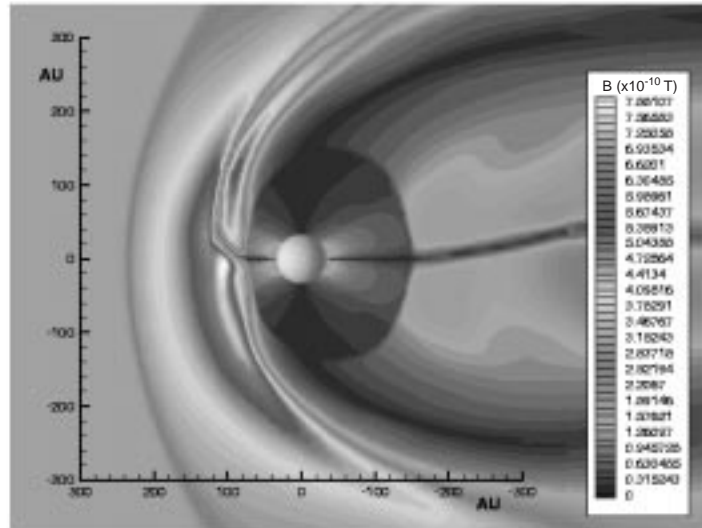
Figure 1. Contours of magnetic field intensity in the north-south meridional plane. From Linde (1998).

Since the heliopause carries electric currents and the average magnetic field across its surface is not equal to zero, there must be a $J \times B$ force applied to it. The magnitude of this force is different in different hemispheres; this explains the shape of the heliopause at the nose. We can also think of this force in terms of magnetic pressure gradients. They are apparently higher in the southern hemisphere (the magnetic wall is steeper there), which results in a distortion of all heliospheric features, including the heliospheric current sheet which is pushed northward.

In the present simulation the upstream location of the termination shock is 78 AU and the bow shock is at 238 AU. The upstream location of the heliopause is somewhat ambiguous due to its complicated shape; in the equatorial plane it is 106 AU. The termination shock position compares very well with an observational estimate of 85 ± 5 AU that results from anomalous cosmic ray energy spectra measurements (Stone *et al.*, 1996) and suggest that a 0.15 nT interstellar magnetic field is sufficient to place the termination shock at this distance from the Sun.
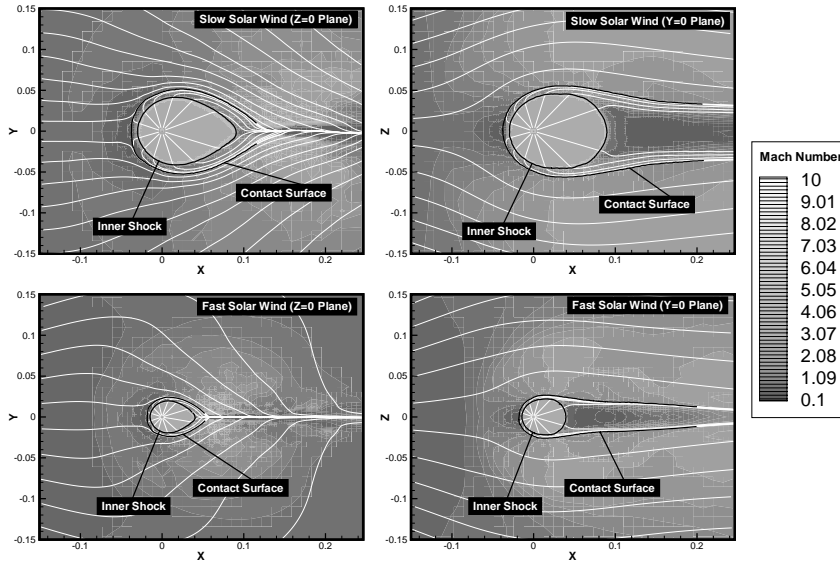
Figure 2. Grey-scale Mach number values and plasma stream lines (white lines) in the inner coma. All distances are given in units of 10^6 km.

3. Comets

We have invested a significant effort into numerical modeling of the interaction of comets with the solar wind. Interestingly, the structure of a cometary 'magneto-sphere' resembles that of the heliosphere. The expanding cometary atmosphere is ionized and becomes similar to the supersonic solar wind, while the real solar wind plays a role similar to the interstellar wind. Just as in the heliosphere, there exists a termination shock, usually called the inner shock, contact surface (an analog of the heliopause) and a bow shock.

We illustrate cometary interactions with the solar wind using the example of a recent bright comet, Hale-Bopp. Previously, we have applied our MHD models to various physical aspects of comets Halley (Gombosi *et al.*, 1996; Häberli *et al.*, 1997; Israelevich *et al.*, 1999) and Hyakutake (Häberli *et al.*, 1997). A complete presentation of our results for Hale-Bopp can be found in Gombosi *et al.* (1999).

Because comet Hale-Bopp's orbit is inclined at a large angle with respect to the ecliptic plane, it was in the fast solar wind for at least part of its trajectory through the inner solar system. Since the properties of the fast solar wind are quite different from those of slow solar wind, the interaction would be different as well.

Figure 2 presents the results of two our simulations, corresponding to these two scenarios. The bow shock in both cases is too far upstream to be seen in these figures (although it is still resolved in our models). The subsolar distance of the

shock is $\sim 1.6 \times 10^6$ km for the slow solar wind and $\sim 1.2 \times 10^6$ km for fast conditions.

The parameters of these two simulations are: IMF magnitude 4.81 nT, IMF angle 24°, solar wind number density 5 cm^{-3}, mean molecular mass of solar wind ions 1 amu, solar wind plasma temperature 10^5 K, speed of the slow solar wind 371 km s^{-1}, speed of the fast solar wind 742 km s^{-1}. Therefore, the Mach number is 10 for the slow solar wind and 20 for the fast. The Alfvénic Mach numbers are 7.9 and 15.8 respectively.

Hale-Bopp was an extremely active comet, with a total gas production rate estimated to be 10^{31} molecules s^{-1}. We have used an ionization scale length of 10^6 km, an ion-neutral momentum transfer collision rate of 1.7×10^{-9} cm^3 s^{-1}, and a mean molecular mass of cometary ions equal to 17 amu.

The interaction between the radially expanding 'ionospheric' plasma and the contaminated, nearly stagnating solar wind flow has been extensively discussed in the past. The formation of a contact surface and an 'inner shock' was predicted theoretically in order to divert the ionospheric plasma flow toward the tail and avoid inter-penetration between the ionospheric and solar wind plasmas (Mendis *et al.*, 1985). Also, as a result of recombination of the shocked ionospheric plasma in the subsolar region, the inner shock can move very close to the boundary separating the two plasma flows (Cravens, 1989). This phenomenon was observed at comet Halley (Goldstein *et al.*, 1989). It was also predicted, that due to the separation of the 'ionospheric' and solar wind plasmas no magnetic field can penetrate inside the contact surface, thus creating a 'diamagnetic cavity'.

Our simulation results are not only completely consistent with the theoretical predictions, but they also reveal many new details of the plasma cavity and near tail regions. It can be seen in Figure 2 that the teardrop shaped inner shock is elongated towards the the tail. On the dayside its subsolar distance is about 3×10^4 km for slow solar wind and $\sim 1.5 \times 10^4$ km for fast solar wind conditions (we note that for comet Halley the comparable distance was about 2 200 km). It is interesting to note that the inner shock is terminated by a Mach disk near the antisolar point. This structure is entirely consistent with the 'point source' nature of the ionospheric plasma flow (Wallis and Dryer, 1976).

Behind the terminator the external plasma flow lines 'converge' toward the sun-comet axis. This 'pinching' effect is well known in planetary magnetospheres and it is a consequence of the pressure gradient perpendicular to the axis of the cometary wake. In effect, the plasma is filling the 'void' created by the cometary obstacle (which basically corresponds to the diamagnetic cavity). The outermost black line in Figure 2 denotes the last solar wind flow line (this separatrix is the contact surface between flow lines in the solar wind and in the ionosphere). This separatrix is the outer edge of the cometary plasma cavity boundary layer. It is interesting to note that the region inside the separatrix narrows considerably on the nightside due to the inflow of the outside plasma into the cometary wake. This converging boundary forces the shocked cometary ionospheric flow into the plasma

tail through a narrow nozzle, and consequently, accelerates the plasma towards the tail.

It is interesting to note that the diamagnetic cavity is basically constrained to the region within the inner shock. Since the ionospheric outflow inside the inner shock is supersonic, the magnetic field cannot diffuse upstream through the inner shock. On the dayside the inner shock is quite close to the inner edge of the cometary plasma cavity boundary layer, and the magnetic field is practically negligible inside this region. Behind the terminator, however, a weak magnetic field penetrates into the region between the inner shock and the cometary plasma cavity boundary layer and this region becomes the inner end of the cometary plasma tail.

4. Jovian Satellites Io and Europa

The two previous examples involved interaction with the interstellar wind and the solar wind, which are superfast. In contrast, the Jovian satellites Io and Europa are immersed in the plasma of the Jovian magnetosphere which is subfast. At the distances of the orbits of these satellites, the magnetospheric plasma is mostly co-rotating with Jupiter. The speed of corotation is usually supersonic, but sub-alfvénic, which results in a completely different magnetospheric interaction for the satellites than that of planets or comets. Many properties characteristic of such an interaction were considered theoretically by Neubauer (1998). The steady-state MHD equations with subsonic inflow are of elliptic type, and therefore, strictly speaking, require characteristic far-field boundary conditions. Implementation of such conditions is a complicated and non-trivial problem, we have avoided it by imposing free-streaming boundary conditions very far from the central body. The typical simulation box used for subalfvénic flows is $600 \times 600 \times 900$ body radii with a typical cell on the edges of the simulation box being about 50 R. At such large distances the numerical viscosity and resistivity (proportional to the cell size) effectively wipe out any disturbance capable of propagating upstream.

The Galileo spacecraft provided us with the first detailed in situ measurements of conditions inside the Jovian magnetosphere. It had several flybys of the large Jovian satellites which have significantly increased our understanding of the physics of subalfvénic interactions. Reproduction and interpretation of the Galileo measurements has been the primary object of our work.

Out of several Io flybys, we have the complete data sets only for December 1995 (Kivelson *et al.*, 1996; Frank *et al.*, 1996). The data of the two recent Galileo Io flybys I24 and I25 are not available yet (and unfortunately, because of hardware problems, no relevant measurements were taken during I25). Therefore, we concentrate on the December 1995 dataset. The details of the model are described by Combi *et al.* (1998). Our model is very similar to that of Linker *et al.* (1998). The most resent modifications to the model include day-night asymmetry for the mass-
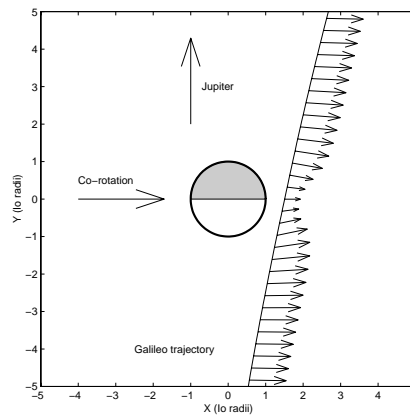
Figure 3. Galileo trajectory close to Io and the plasma velocity vectors along it.

loading, tilt of the upstream magnetic field, and some changes to the treatment of the mass-loading source terms.

Figure 3 shows the geometry of the Galileo December 1995 encounter with Io in the equatorial plane. The night side of Io is shaded. The arrows along the spacecraft trajectory show the plasma velocity calculated in our model.

The reference frame we use in this section is a Cartesian system of reference in which the X axis is parallel to the expected undisturbed plasma velocity (corotation direction), Z is parallel to the Jovian spin axis, and Y completes the right-handed system.

In the present work we have used the same set of the upstream parameters as before, which is representative of the time of the Galileo flyby: upstream plasma density 3500 cm^{-3}, upstream plasma temperature 92 eV, upstream mean molecular mass 22 amu, upstream uniform tilted magnetic field (–300, –75, –1800) nT, corotation flow speed 56.8 km s^{-1}, Alfvénic Mach number 0.4, Mach number 2.2, ratio of specific heats 1.667.

Plasma density and temperature are shown in Figure 4: continuous line is the model and circles are the plasma measurements (Frank *et al.*, 1996). Our model reproduces not only the height and width of the density peak, but the skewness of the data as well. Our conclusion is that this skewness results from the day-night asymmetry. Another manifestation of the day-night differences can be seen in the higher temperature on the day-side (Figure 4, lower panel).

The comparison of the calculated and measured magnetic field components along the Galileo trajectory is presented in Figure 5. In our earlier model, we assumed that the magnetic field was perpendicular to the equatorial plane as a first approximation. In our present model we included the tilt of the magnetic field consistent with the Galileo measurements.

In our model of Io we do not assume any intrinsic magnetic moment for the satellite, all the signature in the magnetic field comes from the mass-loading and
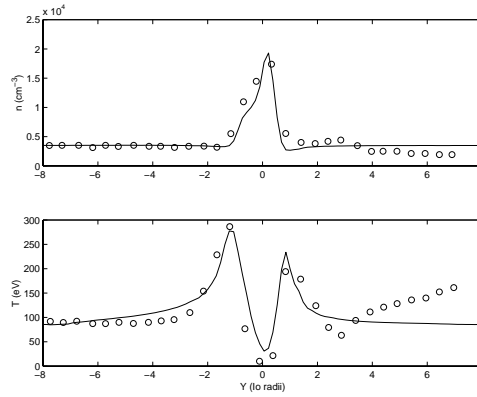
Figure 4. Plasma density and temperature along the Galileo flyby. Continuous line – present model, circles – measurements of Frank *et al.* (1996).
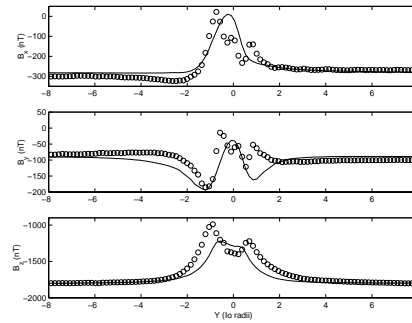

Figure 5. Magnetic field components along the Galileo flyby. Continuous line – present model, circles – measurements of Kivelson *et al.* (1996).

is related to pick-up currents (Goertz, 1980). Our conclusion is that an intrinsic magnetic field for Io is not required to explain Galileo measurements.

As a result of an iterative process, we have adopted the following mass-loading distribution, which allows us to fit well the Galileo measurements:

$$\dot{\rho} = (1 + 6\max(\cos(\chi), 0)) \left(\frac{0.7 \times 10^8}{r^2} + 1.0 \times 10^6 e^{-r/250} \right) \ \text{cm}^{-3}\text{s}^{-1} \qquad (7)$$

Here χ is the sub-solar angle and r is the distance from the center of Io in kilometers. The integrated contributions of the exponential part and of the algebraic part are almost equal to each other (the difference is less than 3%). At the subsolar point the production rate is 6 times larger than on the night-side and the contribution of the entire day-side to the mass-loading is 4 times larger than that of the night-side. The total mass-loading rate is 1.3×10^{28} s^{-1}.

For Europa we have applied our model to the results of the E4 flyby (December 1996). Our model for Europa in many aspects is similar to that for Io. The specific details can be found in Kabin *et al.* (1999). The following upstream parameters
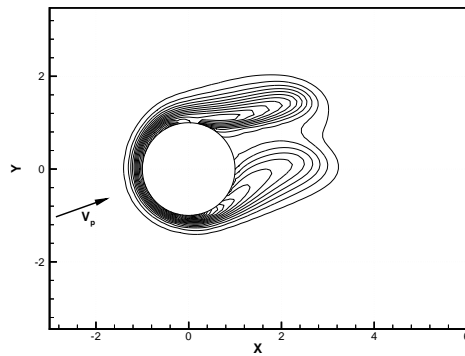
Figure 6. Density contours in the equatorial plane for Europa model. Contours are in 10 cm^{-3} increments; the outermost line corresponds to 40 cm^{-3}. The arrow marked V_p indicates the direction of the plasma flow.
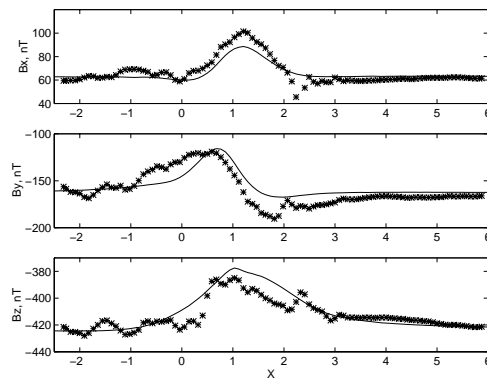

Figure 7. Magnetic field for the Europa model. Crosses are the measurements of Kivelson *et al.* (1997).

were used: plasma density, 35 cm^{-3}; plasma temperature, 90 eV; plasma speed, 90.3 km s^{-1} (corotational value); mean molecular mass, 24 amu; ratio of the specific heats, 1.67; and a uniform tilted Jovian magnetic field with components in the Cartesian frame of reference, (63, –162, –425) nT (tilted 8° with respect to the upstream velocity). These parameters correspond to a sonic Mach number $M = 3.7$ and Alfvénic Mach number $M_A = 0.25$. We have undertaken a long iterative process of adjusting various mass-loading parameters and Europa dipole strength in order to reproduce the Galileo magnetometer measurements of Kivelson *et al.* (1997). In our final version, we used the mass-loading rate of $7 \times 10^{25} \text{ s}^{-1}$. We assumed the mass-loading to be distributed with a scale-height of 175 km on the ram side of the satellite. This value for the scale-height is in agreement with the occultation measurements of Kliore *et al.* (1997).

Figure 6 shows the density distribution in the equatorial plane of Europa. The double-peak structure of the wake agrees well with the electron density inferred

from the plasma frequency measurements of Gurnett *et al.* (1998). Note that the upstream plasma speed is rotated by approximately 20° from the direction of the corotation (the *x*-axis). We found that this rotation improves considerably the comparison with the available measurements. Although it is just a hypothesis at present, it is also supported by the energetic particle measurements of Paranicas *et al.* (1998), as described by Kabin *et al.* (1999).

The reproduction of the magnetic field measurements for the E4 flyby is remarkably good as can be seen in Figure 7. Note, that to achieve this comparison we have assumed an intrinsic dipole moment of 64 nT R_E^3. It has an orientation along the Y axis, very similar to the one predicted by the induction models of (Khurana *et al.*, 1998). Therefore, our model suggests that there can be a conducting layer under the ice surface of Europa although, probably, somewhat thinner than hypothesized by Khurana *et al.* (1998). Most likely, this layer consists of salty water, which may be one of the most interesting discoveries made by the Galileo spacecraft.

5. Mercury

Finally, we present our results for the magnetosphere of the planet Mercury. To the best of our knowledge this is the first three-dimensional MHD model of the magnetosphere of this planet. The details are described in Kabin *et al.* (2000). The plasma flow conditions around Mercury vary greatly depending on the position of the planet along its orbit and on solar activity. As one of the extreme cases we consider Mercury at perihelion, at a distance of about 5.8×10^7 km from the Sun. The average solar wind parameters at this position are: plasma density 73 cm^{-3}, plasma temperature 14 eV, magnetic field 46 nT (in the direction of the nominal Parker spiral), solar wind speed 430 km s^{-1}, ion-acoustic sound speed 74.2 km s^{-1}, Alfvén speed 120 km s^{-1}, mean molecular mass $\sim$ 1 amu, specific heats ratio 1.67. The corresponding Mach number is 5.8 and Alfvénic Mach number 3.6. The Parker's spiral magnetic field forms an angle of 20° with the solar wind direction. We assumed the intrinsic magnetic moment of the planet to be a dipole of 350 nT R_M^3 aligned with the Z axis (Connerney and Ness, 1988). The magnetic field of Mercury is strong enough to form a permanent magnetosphere under typical solar wind conditions.

Both Earth's and Mercury's magnetospheres result from the interaction of the solar wind with a dipole roughly perpendicular to the direction of the solar wind. This is the explanation for the similarities in the basic structure of the two magnetospheres. The differences arise because the typical solar wind parameters are different and the magnetic field of Mercury is much smaller than that of Earth.

Figure 8 shows the 3D magnetic field lines near Mercury. One can see from Figure 8 that the magnetosphere of Mercury is very 'open'. As expected, the polar cap is asymmetric and is significantly larger on the night side than on the day side. The total area of the northern polar cap is about 2 R_M^2. The last closed field-lines
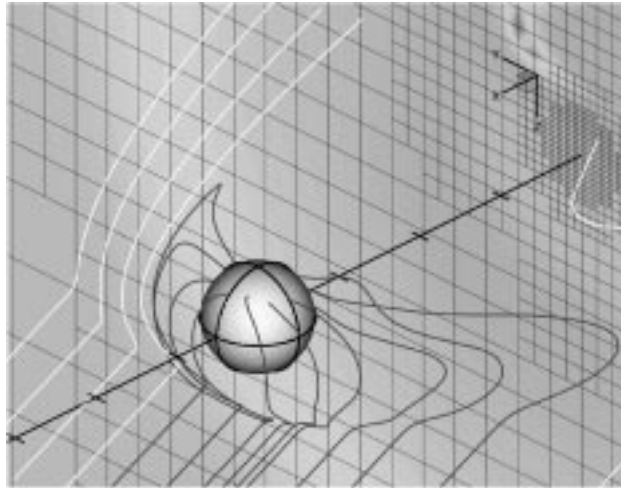
Figure 8. Three-dimensional structure of the magnetosphere of Mercury for the nominal Parker spiral. The background plane is located 8 R_M downstream. The X axis is shown by a black line with tick-marks every 2 R_M. On the surface of Mercury are indicated the equator and the subsolar and terminator meridians. The dark grey field lines are connected to the northern hemisphere of Mercury and the white field lines are open on both sides.

cross the surface of the planet at about 52° north on the day-side, and at 18° on the night-side. For comparison, a typical boundary between closed and open field lines is at 75° at Earth and at around 70° at Jupiter. Our value for the polar cleft latitude is close to, although somewhat larger than that suggested by Ness (1979), Russell *et al.* (1988), and Ogilvie *et al.* (1977) who estimated it to be around 50° − 57° on the dayside and 25° − 35° on the night side.

A very interesting question is if the direct interaction of the solar wind with the surface of Mercury is possible. In order to investigate this possibility we have increased the solar wind speed and pressure (keeping the Mach number constant) until the solar wind was able to reach the surface of the planet directly and the whole day-side magnetosphere was pushed under the surface. In this case a 'bald spot' forms around the subsolar point. The discussion of this simulation can be found in Kabin *et al.* (2000).

The parameters at which the direct interaction of the solar wind with Mercury was found in our model are: solar wind speed 1100 km s^{-1} and solar wind temperature 100 eV. The density and the direction and IMF intensity were kept the same as for the nominal Parker spiral conditions. While cases of a temperature increase in the solar wind by a factor of 7 may be found in measurements, the required increase in the solar wind speed is well above the typical variations. Thus, we may conclude that the direct interaction of the solar wind with the surface of Mercury is a relatively unusual feature. It is still possible, however, if the solar wind density increases at the same time as temperature and speed. A simple equation for pressure balance suggests that if the density of the solar wind will increase by a factor of

9 (which is not that uncommon) direct interaction may occur even at a solar wind speed of 430 km s^{-1}.

6. Conclusions

In this paper we presented three-dimensional MHD models for several very different space environments: the heliosphere, comets, the Jovian satellites Io and Europa and the planet Mercury. In spite of many differences, all the models had a unifying base – the equations of ideal magnetohydrodynamics. Although our MHD models have been rather successful for all these applications, several non-ideal MHD effects are important and should be treated properly by the next generation of models. These include (but are not limited to) the need for a separate description of electron and ion fluids (Hall MHD), physical resistivity and viscosity, and deviations from thermal equilibrium. The last aspect, in principle, requires switching from the fluid description to a kinetic one. However, it is unlikely that fully kinetic models will replace fluid calculations any time soon – for 3D problems they still seem to be prohibitively expensive in terms of computer power. An approach utilizing higher moment closures may be sufficient for many purposes. The first step will probably be to replace scalar pressure with a complete pressure tensor.

Finally, we would like to stress that the advancement of numerical models should go hand in hand with expanding and improving the available data-base of measurements. Nothing is more stimulating for the modeling work than availability of new (preferably enigmatic) measurements. On the other hand, models can predict new effects which will encourage experimentalists to be perform more detailed new measurements to investigate yet undiscovered physical phenomena.

Acknowledgements

References

Baranov, V.B., Izmodenov, V.V. and Malama, Y.G.: 1998, On Distribution Function of H-atoms in the Problem of the Solar Wind Interaction with the Local Interstellar Medium, *J. Geophys. Res.* **103**, 9575–9578.

Combi, M.R., Kabin, K., Gombosi, T.I., De Zeeuw, D. and Powell, K.: 1998, Io's plasma environment during the Galileo flyby: Global three-dimensional MHD modeling with adaptive mesh refinement, *J. Geophys. Res.* **103**, 9071–9081.

Connerney, J.E.P. and Ness, N.F.: 1988, Mercury's magnetic field and its interior, in: F. Vilas, C.R. Chapman and M.S. Matthews (eds.), *Mercury*, The University of Arizona Press, pp. 494–513.

Cravens, T.E.: 1989, A magnetohydrodynamical model of the inner coma of comet Halley, *J. Geophys. Res.* **94**, 15,025–15,040.

Frank, L.A., Paterson, W.R., Ackerson, K.L., Vasyliunas, V.M., Coroniti, F.V. and Bolton, S.J.: 1996, Plasma observations at Io with the Galileo spacecraft, *Science* **274**, 394–395.

Frisch, P.C.: 1996, LISM Structure – Fragmented Superbubble Shell, *Space Sci. Rev.* **78**, 213–222.

Goertz, C.K.: 1980, Io's interaction with the plasma torus, *J. Geophys. Res.* **85**, 2949–2956.

Goldstein, B.E., Altwegg, K., Balsiger, H., Fuselier, S.A., Ip, W.-H., Meier, A., Neugebauer, M., Rosenbauer, H. and Schwenn, R.: 1989, Observations of a shock and a recombination layer at the contact surface of comet Halley, *J. Geophys. Res.* **94**, 17,251–17,257.

Gombosi, T.I., De Zeeuw, D.L., Häberli, R.M. and Powell, K.G.: 1996, Three-dimensional multiscale MHD model of cometary plasma environments, *J. Geophys. Res.* **101**, 15,233–15,253.

Gombosi, T.I., Hansen, K.C., De Zeeuw, D.L., Combi, M.R. and Powell, K.G.: 1999, MHD simulation of comets: the plasma environment of comet Hale-Bopp, *Earth, Moon and Planets* **79**, 179–207.

Groth, C.P.T., De Zeeuw, D.L., Powell, K.G., Gombosi, T.I. and Stout, Q.F.: 1999, A parallel solution-adaptive scheme for ideal magnetohydrodynamics, in: *Proc. AIAA 14th Computational Fluid Dynamics Conference*.

Gurnett, D.A., Kurth, W.S., Roux, A., Bolton, S.J., Thomsen, E.A. and Groene, J.B.: 1998, Galileo plasma wave observations near Europa, *Geophys. Res. Lett.* **25**, 237–240.

Häberli, R.M., Combi, M.R., Gombosi, T.I., De Zeeuw, D.L. and Powell, K.G.: 1997, Quantitative analysis of H_2O^+ coma images using a multiscale MHD model with detailed ion chemistry, *Icarus* **130**, 373–386.

Häberli, R.M., Gombosi, T.I., De Zeeuw, D.L., Combi, M.R. and Powell, K.G.: 1997, Modeling of cometary x-rays caused by solar wind minor ions, *Science* **276**, 939–942.

Israelevich, P.L., Gombosi, T.I., Ershkovich, A.I., De Zeeuw, D.L., Neubauer, F.M. and Powell, K.G.: 1999, The induced magnetosphere of comet Halley, 4.: Comparison of *in situ* observations and numerical simulations, *J. Geophys. Res.* **104**, 28,309–28,319.

Kabin, K., Combi, M.R., Gombosi, T.I., Nagy, A.F., De Zeeuw, D.L. and Powell, K.G.: 1999, On Europa's magnetospheric interaction: An MHD simulation of the E4 flyby, *J. Geophys. Res.* **104**, 19,983–19,992.

Kabin, K., Gombosi, T.I., De Zeeuw, D.L. and Powell, K.G.: 2000, Interaction of Mercury with the solar wind, *Icarus* **143**, 397–406.

Khurana, K.K., Kivelson, M.G., Stevenson, D.J., Schubert, G., Russell, C.T., Walker, R.J. and Polanskey, C.: 1998, Induced magnetic fields as evidence for subsurface oceans in Europa and Callisto, *Nature* **395**, 777–780.

Kivelson, M.G., Khurana, K., Joy, S., Russell, C., Southwood, D., Walker, R.J. and Polanskey, C.: 1997, Europa's magnetic signature: Report from Galileo's pass on 19 December 1996, *Science* **276**, 1239–1241.

Kivelson, M.G., Khurana, K.K., Walker. R.J., Warnecke, J., Russell, C.T., Linker, J.A., Southwood, D.J. and Polanskey, C.: 1996, Io's interaction with the plasma torus: Galileo magnetometer report, *Science* **274**, 396–398.

Kliore, A.J., Hinson, D., Flasar, F., Nagy, A. and Cravens, T.: 1997, The ionosphere of Europa from Galileo radio occultations, *Science* **277**, 355–358.

Linde, T.J.: 1998, *A Three-Dimensional Adaptive Multifluid MHD Model of the Heliosphere*, Ph.D. thesis, University of Michigan, Ann Arbor, Michigan.

Linde, T.J., Gombosi, T.I., Roe, P.L., Powell, K.G. and De Zeeuw, D.L.: 1998, The Heliosphere in the Magnetized Local Interstellar Medium: Results of a 3D MHD Simulation, *J. Geophys. Res.* **103**, 1889–1904.

Linker, J.A., Khurana, K.K., Kivelson, M.G. and Walker, R.J.: 1998, MHD simulation of Io's interaction with the plasma torus, *J. Geophys. Res.* **103**, 19,867–19,877.

Mendis, D.A., Houpis, H.L.F. and Marconi, M.L.: 1985, The physics of comets, *Fund. Cosmic Phys.* **10**, 1–380.

Ness, N.F.: 1979, The magnetosphere of Mercury, in: C. Kennel, L.J. Lanzerotti and E.N. Parker (eds.), *Solar system plasma physics. Vol II*, North Nolland, Amsterdam, pp. 183–206.

Neubauer, F.M.: 1998, The sub-Alfvénic interaction of the Galilean satellites with the Jovian magnetosphere, *J. Geophys. Res.* **103**, 19,834–19,866.

Ogilvie, K.W., Scudder, J.D., Vasyliunas, V.M., Hartle, R.E. and Siscoe, G.L.: 1977, Observations at the planet Mercury by the plasma electron experiment: Mariner 10, *J. Geophys. Res.* **82**, 1807–1824.

Paranicas, C., Cheng, A.F. and Williams, D.J.: 1998, Inference of Europa's conductance from the Galileo energetic particles detector, *J. Geophys. Res.* **103**, 15,001–15,007.

Powell, K.G., Roe, P.L., Linde, T.J., Gombosi, T.I. and De Zeeuw, D.L.: 1999, A Solution-Adaptive Upwind Scheme for Ideal Magnetohydrodynamics, *J. Comput. Phys.* **154**, 284–309.

Russell, C.T., Baker, D.N. and Slavin, J.A.: 1988, The magnetosphere of Mercury, in: F. Vilas, C.R. Chapman and M.S. Matthews (eds.), *Mercury*, The University of Arizona Press, pp. 514–561.

Stone, E.C., Cummings, A.C. and Webber, W.R.: 1996, The distance to the solar wind termination shock in 1993 and 1994 from observations of anomalous cosmic rays, *J. Geophys. Res.* **101**, 11,017–11,025.

Stout, Q.F., De Zeeuw, D.L., Gombosi, T.I., Groth, C.P.T., Marshall, H.G. and Powell, K.G.: 1997, Adaptive blocks: A high-performance data structure, in: *Proc. Supercomputing '97*.

Wallis, M.K. and Dryer, M.: 1976, Sun and comets as sources in an external flow, *Astrophys. J.* **205**, 895–899.